APSB
Acta Pharmaceutica Sinica B
2021
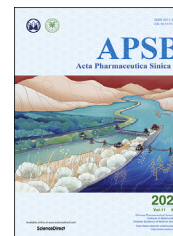
ORIGINAL ARTICLE

Layered dissolving microneedles as a need-based delivery system to simultaneously alleviate skin and joint lesions in psoriatic arthritis

Kaiyue Yu, Xiuming Yu, Sisi Cao, Yixuan Wang, Yuanhao Zhai, Fengdie Yang, Xiaoyuan Yang, Yi Lu, Chuanbin Wu, Yuehong Xu*

School of Pharmaceutical Sciences, Sun Yat-sen University, Guangzhou 510006, China

Abstract   Psoriatic arthritis (PsA) is a complicated psoriasis comorbidity with manifestations of psoriatic skin and arthritic joints, and tailoring specific treatment strategies for simultaneously delivering different drugs to different action sites in PsA remains challenging. We developed a need-based layered dissolving microneedle (MN) system loading immunosuppressant tacrolimus (TAC) and anti-inflammatory diclofenac (DIC) in different layers of MNs, *i.e.,* TD-MN, which aims to specifically deliver TAC and DIC to skin and articular cavity, achieving simultaneous alleviation of psoriatic skin and arthritic joint lesions in PsA. *In vitro* and *in vivo* skin permeation demonstrated that the inter-layer retained TAC within the skin of ∼100 μm, while the tip-layer delivered DIC up to ∼300 μm into the articular cavity. TD-MN not only efficiently decreased the psoriasis area and severity index scores and recovered the thickened epidermis of imiquimod-induced psoriasis but also alleviated carrageenan/kaolin-induced arthritis even better than DIC injection through reducing joint swelling, muscle atrophy, and cartilage destruction. Importantly, TD-MN significantly inhibited the serum TNF-α and IL-17A in psoriatic and arthritic rats. The results support that this approach represents a promising alternative to multi-administration of different drugs for comorbidity, providing a convenient and effective strategy for meeting the requirements of PsA treatment.

1. Introduction

Psoriasis is an immune-mediated chronic inflammatory skin disease that affects 2%−5% of the population worldwide[1]. The clinical manifestation of skin psoriatic lesions is characterized by erythema, scales, and inflammatory plaques, which are generally located on the skin and joints, such as the elbows and knees[2]. These plaques are clearly demarcated from normal skin and attributed to excessive proliferation and abnormal differentiation of keratinocytes leading to epidermal thickening and parakeratosis[3]. This pathological process is accompanied by dermal angiogenesis resulting in a deep red coloration of plaques and acceleration of inflammatory cell influx along the vascularity into the skin, further increasing inflammation[4]. Approximately 13%−25% of psoriasis patients present with chronic inflammatory joint disease, recognized as psoriatic arthritis (PsA)[5,6]. PsA is a complicated comorbidity with simultaneous psoriasis and arthritis symptoms. Inflammatory lesions consist of skin psoriatic lesions and articular cartilage erosion caused by synovitis[7], which leads to high distress and severe pain for patients. Therefore, effective treatment for PsA requires concomitant drugs considering various lesions at the same time, especially those that alleviate skin psoriasis and arthritic symptoms.

PsA is incurable and easy to relapse. Although state-of-the-art treatments for PsA include the application of phosphodiesterase-4 enzyme inhibitors, such as apremilast, inhibitors of Janus kinase (JAK)/STAT pathways, and monoclonal antibodies, there is not yet a curable medication for PsA, and numerous patients present a lack of efficacy or contraindications to these drugs[8]. In addition, their high cost hinders their availability to patients. Topical treatment remains important for psoriasis and PsA because the site of action is direct[9,10]. Topical therapeutic drugs for skin psoriatic lesions include emollients, vitamin D analogs, retinoic acid, glucocorticoids, and immunosuppressants[1]. Of these, the immunosuppressant tacrolimus (TAC) has been proven to have notable therapeutic effects on immune-mediated skin disorders, such as psoriasis, with lower side effects[11−13], as well as demonstrable anti-arthritic effects following the failure of methotrexate treatment[14]. However, the challenges of topical TAC application to treat psoriasis is poor drug permeability through psoriatic skin, abnormal thickened epidermis from psoriasis and high hydrophobicity and molecular weight (822.05 Da) of TAC hinder its permeation. Apart from the treatment of psoriasis, the European League Against Rheumatism (EULAR) and Group for Research and Assessment of Psoriasis and Psoriatic Arthritis (GRAPPA) recommendations from 2015 for the management of PsA with pharmacological therapies mainly consist of nonsteroidal anti-inflammatory drugs (NSAIDs), disease-modifying antirheumatic drugs (DMARDs), and glucocorticoids[10,15]. NSAIDs effectively inhibit cyclooxygenase activity and prostaglandin synthesis, thereby providing a potent anti-inflammatory effect. Although NSAIDs significantly alleviate the pain and swelling induced by arthritis, they have no obvious therapeutic effect on skin lesions[16].

Moreover, oral administration of NSAIDs is associated with gastrointestinal toxicity[17]. Topical administration of diclofenac (DIC), a potent NSAID[18], has been widely used to treat arthritis. However, its topical application needs to be able to penetrate the skin and permeate to the target site of intra-articular in quantities sufficient to exert a therapeutic effect; if necessary, the intra-articular injection of NSAIDs has been applied but shows a poor patient compliance[19,20].

Microneedles (MNs) are interesting drug delivery technique enhancement, having the combined advantages of noninvasive (percutaneous delivery) and invasive (administration by injection) drug delivery[21]. They have been primarily designed to facilitate percutaneous drug delivery and have now progressed into diverse organs and tissues[22]. MNs efficiently deliver drugs including insulin, vaccines, and a diverse range of high- and low-molecular weight compounds for diabetes mellitus[23], vaccination[24], skin diseases, such as psoriasis and skin cancer[25−29], and arthritis[22,30]. MNs aid drug permeation by creating numerous microchannels in the stratum corneum (SC) with negligible pain and tissue damage[31]. The major MN types include solid MNs, coated MNs, hollow MNs, dissolving MNs, and hydrogel-forming MNs[32]. Dissolving MNs are fabricated by biodegradable and biocompatible natural polymers such as hyaluronic acid (HA), dextran, chitosan, silk fibroin, or synthetic polymers such as polyvinyl pyrrolidone (PVP), polyvinyl alcohol (PVA), polylactic acid (PLA), and poly-D,L-lactide-coglycolide (PLGA)[33]. Upon insertion into the skin, dissolving MNs become fully dissolved and the drug encapsulated within the polymeric matrix is released in a sustained manner, which is beneficial for controlling drug release, and enhancing drug permeability. In addition, dissolving MNs can stimulate epidermal cell proliferation and skin collagen production thus accelerating wound healing and improving skin quality[34]. Dissolving MNs have been demonstrated to deliver small molecule and macromolecule drugs within the skin or deeper into the underlying tissues with improved efficiency. However, most work on MNs has centered on monotherapy for one lesion site, leaving MN-based drug delivery to multiple lesion sites, such as PsA, relatively unexplored. PsA poses unique challenges for the implementation of MNs for drug delivery; its lesions both on the skin and in the articular cavity require MNs tailored for delivering different drugs to different action sites simultaneously.

Herein, we developed a need-based layered dissolving MN system loading TAC and DIC in different layers, i.e., TD-MN, to specifically deliver TAC and DIC to the skin and articular cavity, achieving simultaneous alleviation of psoriatic skin and arthritic joint lesions in PsA. Layered MNs consisting of a pedestal, an inter-layer, and a tip-layer were fabricated. TAC was loaded into the inter-layer of the MNs with the solubilization of nicotinamide (NIC), while DIC was loaded into the tip-layer of the MNs. After MN insertion, the tip-layer first penetrated the stratum corneum, further pierced through the epidermis and reached a deeper site. The loaded DIC preferentially permeated into the articular cavity

to treat arthritis, thereby avoiding adverse gastrointestinal effects and liver first-pass effects caused by oral administration, replacing intra-articular injection with better patient compliance. While the inter-layer penetrated the SC and reached the epidermis, and the loaded TAC was mainly retained within the epidermis to treat skin psoriatic lesions on site. The MN layer-loaded and site-specific delivery of TAC and DIC is anticipated to simultaneously alleviate skin psoriasis and joint arthritis and provide a new approach for PsA treatment.

2. Materials and methods

2.1. Materials

Tacrolimus (TAC) was purchased from Teva Czech Industries, S.R.O. (Opava-Komarov, Czech Republic). Diclofenac sodium (DIC), λ-carrageenan, and kaolin were purchased from Macklin Inc. (Shanghai, China). Hyaluronic acid (HA, 30−100 kDa) was purchased from Shangdong Freda Biotechnology Co., Ltd. (Linyi, China). Dextran (40 kDa) was obtained from Aladdin (Shanghai, China). Polyvinylpyrrolidone (PVP) K17 was a gift from BASF (Ludwigshafen, Germany). Nicotinamide (NIC) was a gift from Guangzhou Changlong Technology Co., Ltd. (Guangzhou, China). Rhodamine B (RhB) and coumarin 6 (C6) were obtained from Sigma−Aldrich (St. Louis, MO, USA).

Sprague−Dawley (SD) rats were obtained from the Experimental Animal Center of Sun Yat-sen University (Guangzhou, China). Animals were housed under specific pathogen-free conditions at constant levels of humidity and temperature on 12-h light/dark cycles, and provided with food and water ad libitum. All work undertaken with animals was in accordance with the Principles of Laboratory Animal Care and Use in Research published by the Chinese Ministry of Health, and the protocols were approved by the Institutional Animal Care and Use Committee of Sun Yat-sen University, Guangzhou, China.

2.2. Formulation of layered MNs

2.2.1. Preparation of the drug-loaded MN matrix solution
Previously, we optimized MN matrix solution to fabricate HA-based dissolving MNs[35]. In this study, formulation of the matrix solution of different layers was modified considering the loaded drug and mechanical strength of the MNs (Table 1). Briefly, a blend of HA, dextran, and PVP K17 at a weight ratio of 1/4/1 was dissolved in distilled water, and then DIC or RhB was added and dissolved uniformly to obtain the tip-layer solution containing DIC or RhB at 1% (w/w). Similarly, the inter-layer solution loading of 0.1% (w/w) TAC or C6 and the pedestal solution were obtained based on Table 1. NIC in the inter-layer solution was used to solubilize TAC and enhance the mechanical strength of interlayer based on our previous studies[36,37].

Table 1 Formulation of matrix solution of different layers in layered MNs.

Matrix solution	HA (w/v)	Dextran (w/v)	PVP K17 (w/v)	NIC (w/v)	Drug (w/w)
Tip-layer	10%	40%	10%	—	1% DIC
Inter-layer	10%	35%	15%	20%	0.1% TAC
Pedestal	30%	30%	10%	—	—

−Not applicable.

2.2.2. Fabrication of the MNs
A master mold containing 144 (12 × 12) MNs, 600 μm high and 200 μm in base width, was made of brass using the micromilling technique. Polydimethylsiloxane (PDMS) was poured into the master mold and cured at 80 °C for 2 h to inversely replicate the metal MN. Then, after removing the master mold, the PDMS mold was obtained and used to fabricate the layered MNs.

The fabrication of the layered MNs is summarized in Fig. 1A. First, approximately 35 mg of tip-layer solution was pipetted into the PDMS mold and subjected to centrifugation (Beckman Coulter, Allegra-30R, Indianapolis, IN, USA) at 4000 rpm for 20 min until the solution entered the PDMS mold microcavities. The PDMS mold loaded with tip-layer solution was dried under vacuum for 2 h until the tip-layer of needle formed. Second, approximately 35 mg of inter-layer solution was casted onto the tip-layer surface, centrifuged (Beckman Coulter) as above, and dried under vacuum for 2 h to form the inter-layer of MNs. Finally, the pedestal solution of 130 mg was added to cover the inter-layer surface, smoothed using a spatula, and then centrifuged (Beckman Coulter) at 3000 rpm for 10 min to form a pedestal. The filled mold was dried overnight at 4 °C, and the TAC and DIC co-loaded layered MNs (TD-MN) was obtained by peeling off the PDMS mold. In addition, layered MNs only loading DIC in the tip-layer of needles (DIC-MN), layered MNs only loading TAC in the inter-layer of needles (TAC-MN) were fabricated with the same procedure as TD-MN, while unlayered MNs loading a mixture of TAC and DIC into the needles (MIX-MN) were fabricated with the mixture of tip-layer and inter-layer solution. TD-MN and MIX-MN contained equal amounts of TAC (∼31 μg/patch) and DIC (∼330 μg/patch), while TAC-MN contained TAC (∼31 μg/patch) alone and DIC-MN contained DIC (∼330 μg/patch) alone.

2.3. Characterization of the layered MNs

2.3.1. Morphology and structure of the MNs
The surface morphology of the layered MNs was observed by using a digital optical microscopy (Paulone, XWJ001, Shenzhen, China) and scanning electron microscopy (SEM, Zessi EVO MA10, Jena, Germany). To visualize the layered structure of the MNs, fluorescent probe-loaded layered MNs were prepared and imaged by confocal laser scanning microscopy (CLSM, Zessi, LSM 710, Jena, Germany). Coumarin 6 (C6) and rhodamine B (RhB) were used as fluorescent probes to mimic lipophilic TAC and hydrophilic DIC, respectively.

2.3.2. Drug loading and mechanical strength of the MNs
The MN patch was dissolved in 30% (v/v) methanol aqueous solution. The content of TAC and DIC in the MNs was determined with high performance liquid chromatography (HPLC).

The mechanical strength of the MNs was determined using a TAXT-Plus texture analyzer (Stable Micro Systems, Surrey, UK). The MN patch was fixed onto the test station and an axial compression load was applied to the MN patch by the test probe at a rate of 1 mm/s. The force was recorded by the texture analyzer, as a result of mechanical strength, until a preset displacement of 600 μm was reached or the needles broke.

2.4. Insertion depth of the MNs

2.4.1. In vitro parafilm and skin insertion
To assess the insertion properties of the layered MNs, a Parafilm M® sheet was folded into a ten-layer film as a skin simulant[38,39].

The MN patch was attached to the movable test probe, and the probe pressed onto the folded parafilm at the required force of 30 N and held for 5 min. After insertion, the MN patch was removed from the parafilm sheet, and the number of micro-channels created by the MN in each layer was counted under a digital optical microscope (Paulone). To further confirm the depth of MN insertion into the skin *in vitro*, full-thickness rat skin was securely fixed on a flat surface, and the MN patch was inserted into the skin with a force of 30 N for 5 min. Optical coherence tomography (OCT) images of MN insertion site were recorded in real time using an OCT microscope (TEK SQRAY HSO-2000, Shenzhen, China).

2.4.2. *In vivo skin insertion*

The fluorescent probes C6 and RhB were chosen as alternative drugs toTAC and DIC, respectively, and loaded into layered MNs. A SD rat was anaesthetized and layered MN patch was inserted into the rat skin with a force of 30 N for 5 min and followed by covering with an adhesive tape (Scotch® Transparent Tape, 3M Corporate, St. Paul, MN, USA) for 30 min. Thereafter, the treated rat was euthanized, and the treated skin was excised and spread on the microslide. To visualize the distribution of C6 and RhB at different depths, the microslide was observed by CLSM (Zessi). Z stacks of the skin samples were taken from the SC to the dermis for layer-by-layer scanning. The skin surface ($z = 0$ μm) was defined as the imaging plane of the SC surface. To generate an *xz*-section, a horizontal line was "drawn" across a region of interest in the $z = 0$ μm *xy*-plane and was then "optically sliced" through the digitized image data of the successive *xy*-sections. Imaris (Imaris 6.2, Bitplane, South Windsor, CT, USA) was used for 3D reconstruction of serial sections.

2.5. *Skin permeation of the MNs*

2.5.1. *In vitro skin permeation*

SD rats were anesthetized, and the hair on the skin of the knee joint was carefully shaved off with razor and further removed with depilatory cream (Silk & Fresh, Veet, France). After 24 h of recovery, the treated rats were euthanized, and the skin of the

knee joint was excised, the subcutaneous tissues were removed surgically, and the skin of the knee joint was rinsed with normal saline. *In vitro* skin permeation studies were conducted in Franz cells (TK-12A, Kaikai Technology Ltd., Shanghai, China) with a diffusion area of 1.766 cm². The MN patch inserted the skin with a force of 30 N for 5 min and was covered with an adhesive tape. The skin with MN patch inserted was sandwiched between the donor and receiving cells. The receiving cell was filled with 8 mL of receiving medium, and the medium was maintained at 37 ± 0.5 °C in a circulating water bath and stirred at 250 rpm. At predetermined time intervals (0.5, 1, 2, 4, 6, 9, 12, 16, 20 and 24 h), samples were collected, and an equal volume of fresh receiving medium was subsequently supplemented. At the end of the experiments, the skin was demounted from the Franz cell and cleaned, and the TAC and DIC retained in the skin were extracted with methanol. TAC-MN, DIC-MN, and MIX-MN were also used for *in vitro* skin permeation studies. The contents of TAC and DIC in all samples were determined by HPLC.

2.5.2. *In vivo skin permeation*

For *in vivo* skin permeation studies, SD rats were anesthetized with urethane (20%, *w/v*), and the hair on the skin of the knee joint was carefully shaved off with a razor and further removed with depilatory cream (Silk & Fresh). After 24 h of recovery, the rats were randomly divided into four groups, TD-MN, TAC-MN, DIC-MN, and MIX-MN, with six animals in each group. For each animal, an MN patch was inserted into the hairless knee joint skin with a force of 30 N for 5 min and then covered with adhesive tape. After 24 h of *in vivo* permeation, the residual MN patch was peeled off the skin, tape stripping was performed twice to clean the permeated skin, and then the treated skin was excised. The un-permeated TAC and DIC were extracted from the mixture of the residual MN patch and stripped tape, and the amounts of TAC and DIC retained in the excised skin were also extracted with methanol. The drug contents of all samples were determined by HPLC. The permeated TAC and DIC were calculated as the total amount in the MN patch minus the un-permeated and retained.
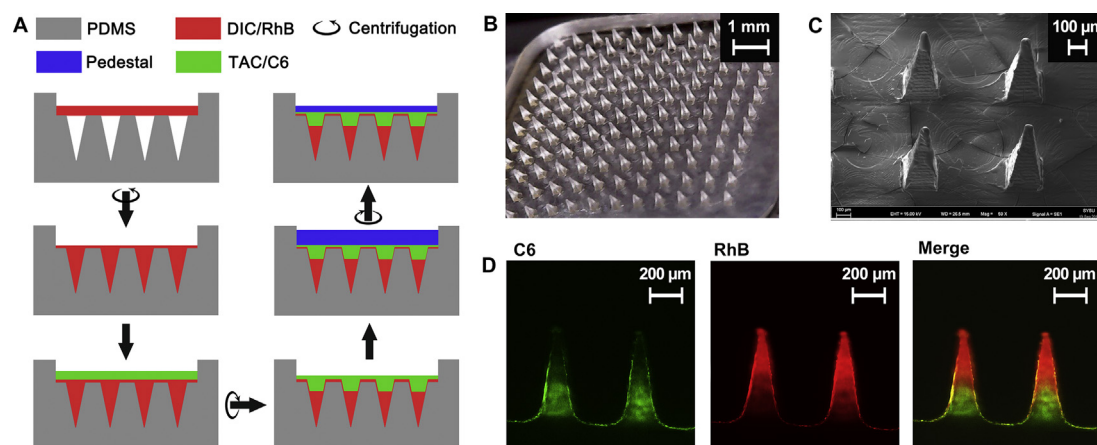
Figure 1   Fabrication and characterization of layered MNs. Schematic fabrication process of layered MNs (A). MN arrays and single needle photographed with digital microscopy (B, scale bar = 1 mm) and scanning electron microscopy (C, scale bar = 100 μm). Layered structure of MNs loading RhB in the tip-layer and C6 in the inter-layer photographed with confocal laser scanning microscopy (D, scale bar = 200 μm).

2.6. In vivo visualization of drug distribution in the articular cavity

An *in vivo* imaging system (IVISR, BERTHOLD, NightOWL II LB983, Stuttgart, Germany) was utilized to visualize the drug distribution in the articular cavity of SD rats. Briefly, layered MNs with RhB alone loaded in the tip-layer of the needle was fabricated. The RhB-loaded MN patch was inserted into the hairless skin of the knee joint of the anesthetic rat with a force of 30 N for 5 min and was then covered with adhesive tape. After the MN patch was adhered for 0.5, 1, 2, 4, 6, 9, 12 and 24 h, respectively, a rat was euthanized, the knee joint skin was removed to eliminate the interference of skin retention, and the fluorescence in the articular cavity was directly observed by IVISR. Animals which were intra-articularly injected with the same amount of normal saline as that of RhB in the MNs were set as the control.

2.7. Pharmacodynamics studies

There is not yet a typical PsA animal model with remarkable symptoms of both skin and joint disease. Interestingly, new methods for constructing PsA animal model have been reported[40]. In the pharmacodynamics studies, SD rats were used to establish an imiquimod (IMQ)-induced psoriasis animal model[41,42] and a λ-carrageenan/kaolin-induced arthritis animal model[43−45]. The treatment results of the two animal models were combined to evaluate the therapeutic effects of the layered MNs on PsA. The pharmacodynamics studies included animal model establishment, treatment after successful modeling, general observations of treatment, histological studies, and serum tumor necrosis factor α (TNF-α) and interleukin 17A (IL-17A) determinations.

2.7.1. Psoriasis model establishment and treatment

The hair in the dorsal skin of SD rats (male, 180−220 g) was shaved off. Commercial IMQ cream (5%, w/w, Hubei Keyi Pharmaceutical Co., Ltd., Wuhan, China) of 0.1 g was topically administered onto the shaved skin for 5 consecutive days. The psoriasis-like skin lesion model was induced, and the psoriatic rats were randomly divided into six groups (n = 6 per group) as follows: IMQ: IMQ-induced rats were treated with normal saline,

erythema, scaling, and skin thickening were scored as follows: 0 (none), 1 (mild), 2 (moderate), 3 (marked), and 4 (very marked). The sum of the three individual scores was defined as the skin inflammation severity score. Moreover, transepidermal water loss (TEWL) was determined with an *S/N* SWL5141 device (Delfin Technologies, Netherlands) to assess the destruction and recovery of skin barrier function.

2.7.2. Arthritis model establishment and treatment

The arthritis model was induced with λ-carrageenan and kaolin in SD rats (male, ∼350 g). Briefly, the rats were anesthetized and the hair on the skin of the knee joint was shaved off. A suspension of 0.1 mL containing 2% (w/v) λ-carrageenan and 4% (w/v) kaolin in sterile normal saline was injected into the synovial cavity of the right knee joint through the patellar ligament, followed by repeated limb extensions and flexions for 15 min to ensure adequate dispersion of the suspension within the joint and to induce articular cartilage abrasion. After 2 days, the right knee joint presented marked swelling compared with the left knee joint. Successful carrageenan/kaolin-induced arthritic rats were randomly divided into 7 groups (n = 6 per group) as follows: The mode group was arthritic rats without treatment, positive control; Blank-MN, DIC-MN, TAC-MN, MIX-MN, and TD-MN groups were arthritic rats treated with Blank-MN, DIC-MN, TAC-MN, MIX-MN, and TD-MN on the skin of the right knee joint region, respectively; and DIC-injection: arthritic rats were treated with intra-articular injection into the right articular cavity of 0.1 mL of normal saline solution containing DIC with the same amount of DIC loaded in MNs. All formulations were administered after successful modeling. For the blank-MN, DIC-MN, TAC-MN, MIX-MN, and TD-MN groups, the MN patch was inserted into the right knee joint with a force of 30 N for 5 min, covered with adhesive tape for 24 h, and then removed. Healthy rats served as the negative control (Control).

The diameters of the left and right knee joints for each animal in each group were measured with a digital micrometer (CD−6 CSX, Mitutoyo Corporation, Kawasaki, Japan) on Days 1, 3, 5, and 7 post-injections of λ-carrageenan and kaolin. The degree of right knee joint swelling was calculated using the following Eq. (1):

$$\text{Swelling degree (\%)} = \frac{\text{Diameter of right knee joint} - \text{Diameter of left knee joint}}{\text{Diameter of left knee joint}} \times 100 \tag{1}$$

positive control; IMQ+Blank-MN: IMQ-induced rats were treated with drug-free layered MNs (Blank-MN); and IMQ+DIC-MN, IMQ+TAC-MN, IMQ+MIX-MN, and IMQ+TD-MN: IMQ-induced rats were treated with DIC-MN, TAC-MN, MIX-MN, or TD-MN, respectively. Healthy rats with shaved dorsal skins were used as the negative control. Except for the controls, each animal in the MN-treated groups was treated with different MN formulations on Day 6. The MN patch was inserted into psoriatic skin with a force of 30 N for 5 min, covered with adhesive tape for 24 h, and then removed.

Throughout psoriasis model establishment and treatment, psoriasis-like skin inflammation severity was visualized and scored on Days 1, 3, 5, 7, 9, and 11 based on the clinical psoriasis area and severity index (PASI)[41,42,46]. Three parameters including

At the end of the experiments, the rats were euthanized, and the gastrocnemius/soleus and tibialis anterior muscles from both legs were isolated. The muscle weight ratio (%) was calculated by comparing the muscle weight of the right hind leg with that of the left hind leg, and this indicated the amyotrophy degree attributed to arthritis. Blood was also collected from each animal and centrifuged (Beckman Coulter) at 2500 rpm for 10 min after standing at room temperature for 4 h. Then, the supernatant serum was collected and stored at −20 °C until use.

2.7.3. Histopathological analysis

At the end of the study, the psoriatic rats were sacrificed to obtain the dorsal skin, and the arthritic rats were sacrificed to obtain the right knee joint. The dorsal skin and the right knee joint were fixed

in 10% (w/v) paraformaldehyde and embedded in paraffin. The sections sliced from the dorsal skin were stained with hematoxylin and eosin (H&E) for pathological evaluation and measurement of the epidermal thickness. The sections of the right knee joint were stained with H&E and safranin O-fast green to evaluate the histological changes of the joint and articular cartilage abrasion.

2.7.4. Detection of serum inflammatory cytokines

The serum TNF-α and IL-17A levels were determined using a rat enzyme-linked immunosorbent assay (ELISA) kit (Abcam, Cambridge, UK) according to the manufacturer's instructions.

2.8. HPLC analysis of TAC and DIC

The contents of TAC and DIC in all samples were determined using HPLC. The HPLC system (Agilent, 1260 series, Santa Clara, CA, USA) consisted of a quaternary pump (G1310A), degasser (G1322A), autosampler (G1329), column thermostat (CO-1000), UV detector (G1314A), and data processing software (Agilent Chem Station for LC systems, Santa Clara, CA, USA). TAC was analyzed with a C8 column (Thermo®, 250 mm × 4.6 mm, 5 μm) with water/isopropyl alcohol/tetrahydrofuran (6/2/2, v/v/v) as the mobile phase at a flow rate of 0.8 mL/min at 55 °C, and a detection wavelength of 220 nm. DIC was analyzed using an XB-C18 column (Ultimate®, 250 mm × 4.6 mm, 5 μm) with methanol/4%acetic acid (v/v) aqueous solution (7/3) as the mobile phase at a flow rate of 1.0 mL/min at 30 °C and a detection wavelength of 276 nm.

2.9. Statistical analysis

All experimental data are expressed as the mean ± standard deviation and were analyzed using one-way analysis of variance (ANOVA) followed by the least significant difference test (LSD) as a post hoc analysis (SPSS version 19.0; SPSS Inc., Chicago, IL, USA). A P value<0.05 was determined to be indicative of statistically significant differences.

3. Results and discussion

3.1. Characterization of the layered MNs

3.1.1. Morphological and structural characterization

The fabricated layered MNs were visualized with digital optical microscopy, SEM, and CLSM. The MN patch consisted of 144 (12 × 12) intact and consecutive needle arrays (Fig. 1B), and each needle showed a triangular pyramidal shape with a height of 600 μm, a base width of 200 μm, and an interval of 400 μm (Fig. 1C). The needles observed with CLSM from tip to pedestal presented the proposed layers including the tip-layer loading hydrophilic RhB and inter-layer loading hydrophobic C6 (Fig. 1D). The layered design of the MNs has the potential to simultaneously deliver different drugs to different sites for the requirements of PsA treatment.

3.1.2. Drug loading and mechanical strength of the MNs

In our layered MN design, the inter-layer was supposed to retain an anti-psoriatic agent within the superficial skin and inhibit psoriasis, the tip-layer was supposed to deliver an anti-inflammatory drug through the skin to the articular cavity and inhibit arthritis, and the MN patch was supposed to provide synergistic anti-psoriatic and anti-inflammatory effects for PsA. The drugs penetrated the skin along the microchannels generated by the MNs. Based on three batches of MN patches determined by HPLC, the drug content in the layered MNs was 31.52 ± 1.78 μg/patch for TAC and 330.79 ± 9.66 μg/patch for DIC. The drug loading of DIC was ∼10-fold that of TAC in each patch, and the ratio of DIC to TAC was consistent with commercial DIC gel and TAC ointment. To overcome the SC barrier and achieve drug delivery through the skin, the MNs must have efficient mechanical strength and rigidity for insertion into skin and penetration through the SC. The mechanical strength of the layered MN patch determined by the texture analyzer was 94.37 ± 3.08 N/patch, more than 90 N/patch (0.6 N/needle), which was strong enough to pierce living skin without being broken based on previous reports[35,47].

3.2. Insertion depth in vitro

We used Parafilm M® as an artificial membrane to mimic the skin to measure the insertion depth of the MNs[38,39]. Layered MNs loaded with TAC and DIC penetrated the artificial membrane and reached the third layer of parafilm. The thickness of each parafilm layer was ∼100 μm, indicating that the insertion depth of layered MN into skin was up to ∼300 μm. The puncture pore ratio created by the needles was 100%, 96.5%, and 48.6% for the first, second, and third layers, respectively (Fig. 2A). In general, the thickness of the SC, viable epidermis, and dermis are 10−20 μm, 50−100 μm, and 1−3 mm, respectively. Thus, the puncture hole ratio suggests that the layered MNs can penetrate through the epidermis and form microchannels from the SC down to dermis. This facilitated the MN percutaneous delivery of the loaded drug to the deep site. To further confirm the depth of MN insertion into skin, the MN patch was inserted into rat skin in vitro, and the MN patch together with the treated skin was imaged with OCT. Fig. 2B shows that the MN needle tips reach a depth of ∼300 μm into the skin and do not break during the insertion process, which was in line with the insertion studies of MN into parafilm and the results reported by Migdadi et al.[38]. The insertion depth was shorter than 600 μm height of the layered MNs mainly due to skin elasticity[47].

3.3. In vivo insertion depth

To further assess the insertion depth of the MNs into the knee joint skin in vivo and the distribution of drugs released from the different layers of the MNs, hairless rat knee joint skin with was punctured by the layered MN patch loaded with C6 in the inter-layer and RhB in the tip-layer. After 30 min of treatment, the skin was scanned layer by layer by CLSM. The insertion depths of C6 and RhB were 3D reconstructed (Fig. 3). The C6 fluorescence was weaker than that of RhB and mainly distributed within the epidermis (0−100 μm), indicating that the drug loaded in the inter-layer of the needles was mainly delivered into the superficial layer of the skin, where the psoriatic lesion was located. Interestingly, the RhB fluorescence was mainly distributed at a depth of 50−250 μm and reached to ∼300 μm. It can be concluded that the drug loaded in the tip-layer of the needles could be delivered through the epidermis and into the dermis of skin, which provides strong support for the hypothesis that the drug loaded in the tip-layer can reach the deeper skin along the microchannel generated by the MNs and subsequently permeate into the articular cavity and exert anti-arthritic effects. These results validated our
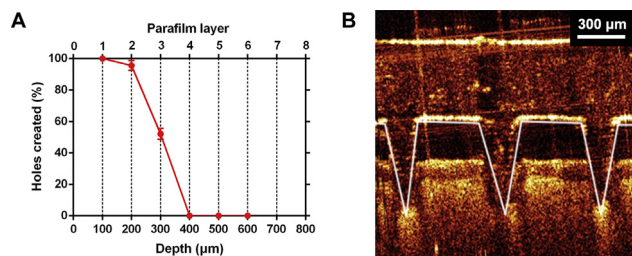
Figure 2 Insertion depth of MNs through Parafilm M® and rat skin *in vitro*. Percentage of holes created and insertion depth of layered MNs in Parafilm M® layers (A). Data are mean±standard derivation of six determinations. Optical coherence tomography image of insertion depth of rat skin treated with layered MNs *in vitro* (B). Scale bar = 300 μm.

hypothesis of delivering different drugs by layered MNs into different skin layers for clinical requirements.

3.4. In vitro and in vivo skin permeation

TD-MN, TAC-MN, DIC-MN, and MIX-MN were examined *in vitro* and *in vivo* permeation studies to assess the percutaneous need-based delivery behaviors of TAC and DIC by the layered MNs.

Figs. 4 and 5 show the drug permeation of different MN formulations through the rat knee skin *in vitro* and *in vivo*, respectively. After 24 h of permeation, TD-MN and TAC-MN presented similar permeation characteristics to TAC *in vitro* and *in vivo*. There was no significant difference between TD MN and TAC-MN in either the TAC cumulative permeated amount or the TAC skin retention. However, the TAC skin retention of TD-MN or TAC-MN was significantly higher than that of MIX-MN ($P < 0.05$). Moreover, the TAC skin retention of TD-MN or TAC-MN was similar to the cumulative permeated amount. TAC loaded into the inter-layer of TD-MN or TAC-MN facilitated its retention in the skin, thereby enhancing the therapeutic effects of TAC on skin psoriatic lesions. Interestingly, the cumulative permeated amount of DIC from TD-MN, DIC-MN, and MIX-MN was 88.03, 75.74, and 53.20 μg/cm^2 *in vitro*, respectively; and 107.69, 100.13, and 49.01 μg/cm^2 *in vivo*, respectively. The DIC skin retention from TD-MN, DIC-MN, and MIX-MN was 4.13, 3.56, and 2.57 μg/cm^2 *in vitro* and 1.79, 1.71, and 1.08 μg/cm^2 *in vivo*, respectively. TD-MN and DIC-MN presented similar permeation characteristics to those of DIC and significantly enhanced DIC permeation compared with MIX-MN ($P < 0.05$). The cumulative permeated amount of DIC from TD-MN was ∼21 and ∼60-fold that of DIC skin retention *in vitro* and *in vivo*, respectively. The majority of DIC loaded in TD-MN could be delivered into the subcutaneous layer of the skin, making it possible to reach the articular cavity and achieve its therapeutic effects on arthritis. The results indicated that DIC loaded in the tip-layer of TD-MN or DIC- MN facilitated its penetration into the skin to deeper tissue. Taken together, the skin permeability of TAC and DIC from the layered MNs was similar to that from TAC-MN or DIC-MN individually and significantly stronger than that from MIX-MN. The Layered MNs loaded with TAC and DIC in different layers is anticipated to kill two birds with one stone by alleviating skin and joint lesions in PsA treatment.

The enhanced TAC retention and DIC penetration of TD-MN may primarily be attributed to the structure of TAC and DIC loaded in the different layers of the layered MNs. In addition, the layered design ensured efficient mechanical strength for the MNs to effectively insert into the skin. The mechanical strength of the layered MNs of 94.37 ± 3.08 N/patch was significantly higher than that of MIX-MN (56.54 ± 2.45 N/patch, $P < 0.05$). The skin is highly elastic, the poor mechanical strength of MIX-MN made them not fully insert into the skin resulting the lower permeation amount and retention amount of drugs.

3.5. In vivo visualization of drug distribution in the articular cavity

To further confirm whether the drug loaded in the tip-layer of the MNs can penetrate the skin and diffuse into the articular cavity, IVISR was utilized to visualize the drug distribution in the articular cavity of the SD rat knee joint. Fig. 6 presents the fluorescence images of the rat knee joints punctured by the layered MNs loaded with RhB alone in the tip-layer of the needles (Fig. 6A), intra-articular injection with RhB solution (Fig. 6B), and the fluorescence intensity with time (Fig. 6C). After treatment with the MNs onto the knee joint for 0.5, 1, 2, 4, 6, 9, 12 and 24 h, the RhB fluorescence in the articular cavity could be quickly observed even if the treated skin was removed after 0.5h, and the fluorescence intensity of RhB increased gradually with time, reached the peak 6 at h, and
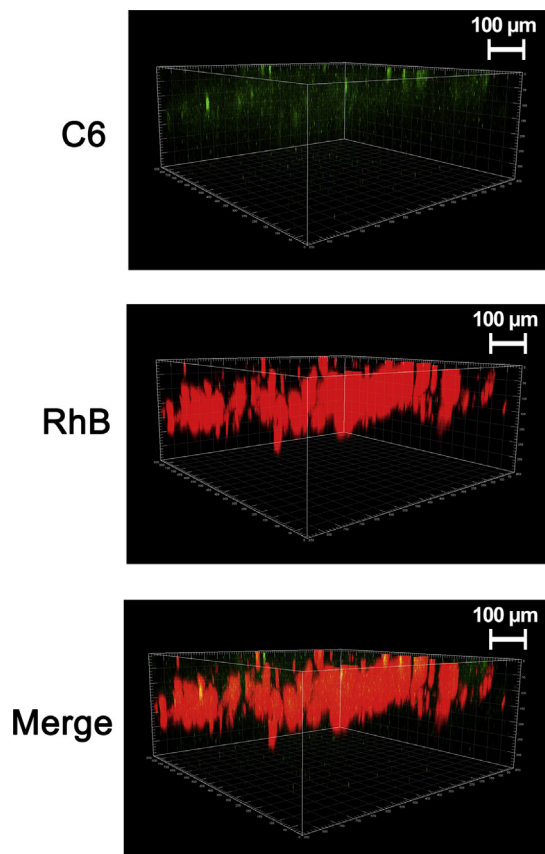
Figure 3 Confocal laser scanning micrographs *via* 3D reconstruction of rat skin treated with fluorescent probes loaded layered MNs *in vivo*. Scale bar = 100 μm.
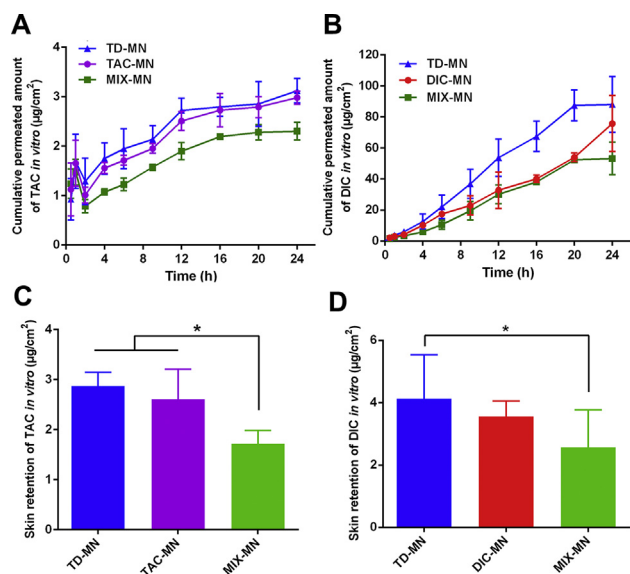
Figure 4 *In vitro* permeation behavior of different MN formulations. Permeation profiles of TAC (A) and DIC (B) through rat skin from different MN formulations. Skin retention of TAC (C) and DIC (D) after 24 h permeation from different MN formulations. Each symbol and bar represented the mean ± standard deviation of six determinations. Significant differences were calculated using ANOVA test (*$P < 0.05$).

remained high until 24 h (Fig. 6A and C). However, the fluorescence intensity was strongest upon the intra-articular injection of RhB solution, decreased gradually with time, became weaker at 4 h post-injection, and remained negligible from 6 to 12 h post-injection
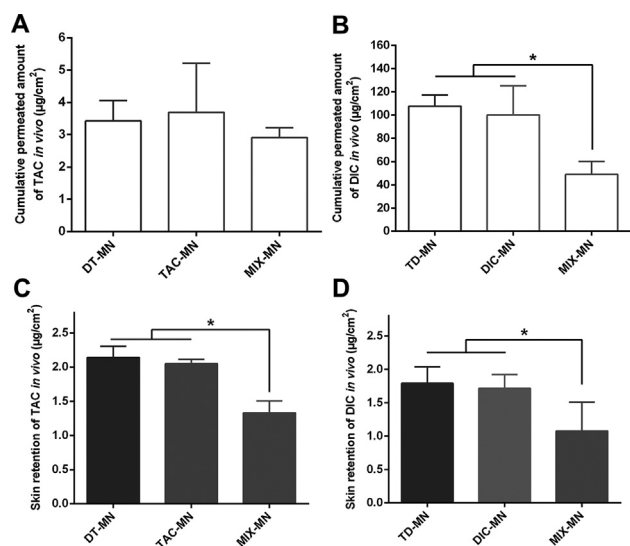
Figure 5 *In vivo* permeation behavior of different MN formulations. Cumulative permeated amount of TAC (A) and DIC (B) through rat skin, and skin retention of TAC (C) and DIC (D) after 24 h permeation from different MN formulations. Each symbol and bar represented the mean ± standard deviation of six determinations. Significant differences were calculated using ANOVA test (*$P < 0.05$).

(Fig. 6B and C). After the skin of the injected position was removed at the time point of 12 h, there was no fluorescence signal in the articular cavity, while the weak fluorescence was present in the skin (Fig. 6B). The negligible fluorescence from 6 h post-injection might be residual RhB in the skin due to needle injection. The results indicate that RhB loaded into the tip-layer of the MNs could penetrate the skin faster and reach the articular cavity, and the layered MNs sustainably delivered the drug into the articular cavity as a drug reservoir and prolonged the residence time of the drug in the articular cavity. Intra-articular injection could immediately deliver the drug into the articular cavity; however, the drug was quickly distributed systemically and then metabolized. Mwangi et al.[48] reported that the fluorescence of labeled 10 kDa dextran in the joint rapidly decayed after intra-articular injection with a joint half-life of 3.26 h, and this short joint residence time was associated with its small molecular weight and joint clearance. Frequent intra-articular injection of DIC with a molecular weight of 318 is necessary for the sustained control of PsA development. Delivering drugs with layered MNs into the articular cavity may be an alternative to intra-articular injection and has the advantage of facilitating long-term sustained release of drugs in the articular cavity, which leads to enhanced patient compliance because long-term treatment is required for PsA.

3.6. Effects of layered MN on psoriatic arthritis treatment

3.6.1. General observations
A schematic diagram of psoriasis model establishment and the treatment protocol is shown in Fig. 7A. Fig. 7B–D respectively presents the representative clinical manifestations, PASI, and TEWL of healthy and psoriatic animals throughout the model establishment and treatment. After consecutive applications of IMQ cream to the rats for 5 days, rat skin displayed typical characteristics of psoriasis-like lesions, including severe erythema with punctate hemorrhage and caducous scales, and obvious skin thickening with wrinkles and raised plaques (Fig. 7B). PASI scores and TEWL values rose to ∼8 and ∼33 g/m²·h (0 and 3.58 ± 0.26 g/m²·h for healthy skin, Fig. 7C and D), respectively. The skin barrier was significantly disrupted due to psoriatic lesions. After treatment with different MN formulations on Day 6 for 24 h, the skin lesions formed scabs, the PASI scores and TEWL values decreased. Throughout treatment, TD-MN and TAC-MN had better anti-psoriatic effects than Blank-MN, DIC-MN, and MIX-MN, while Blank-MN, DIC-MN, and MIX-MN presented comparable results. Reduction of PASI scores and TEWL values represented the healing and recovery extent of skin lesions. By the end of the experiment (Day 11), the PASI scores and TEWL values of the TD-MN- and TAC-MN-treated groups were significantly less than those of the other MN groups ($P < 0.05$), and those of the Blank-MN, DIC-MN, and MIX-MN groups were significantly less than those of the IMQ group ($P < 0.05$). The visible inflammatory signs of psoriatic lesions were significantly ameliorated after TD-MN or TAC-MN treatment, and the skin barrier recovered and was comparable to the negative control (healthy animal). The results were attributed to the facts as follows. First, TAC, a potent immunosuppressant, played a major role in the treatment of psoriasis, while DIC, an NSAIDs, could not have marked anti-psoriatic effects. Second, percutaneous delivery of TAC in the inter-layer of the layered MNs (TD-MN or TAC-MN) obtained
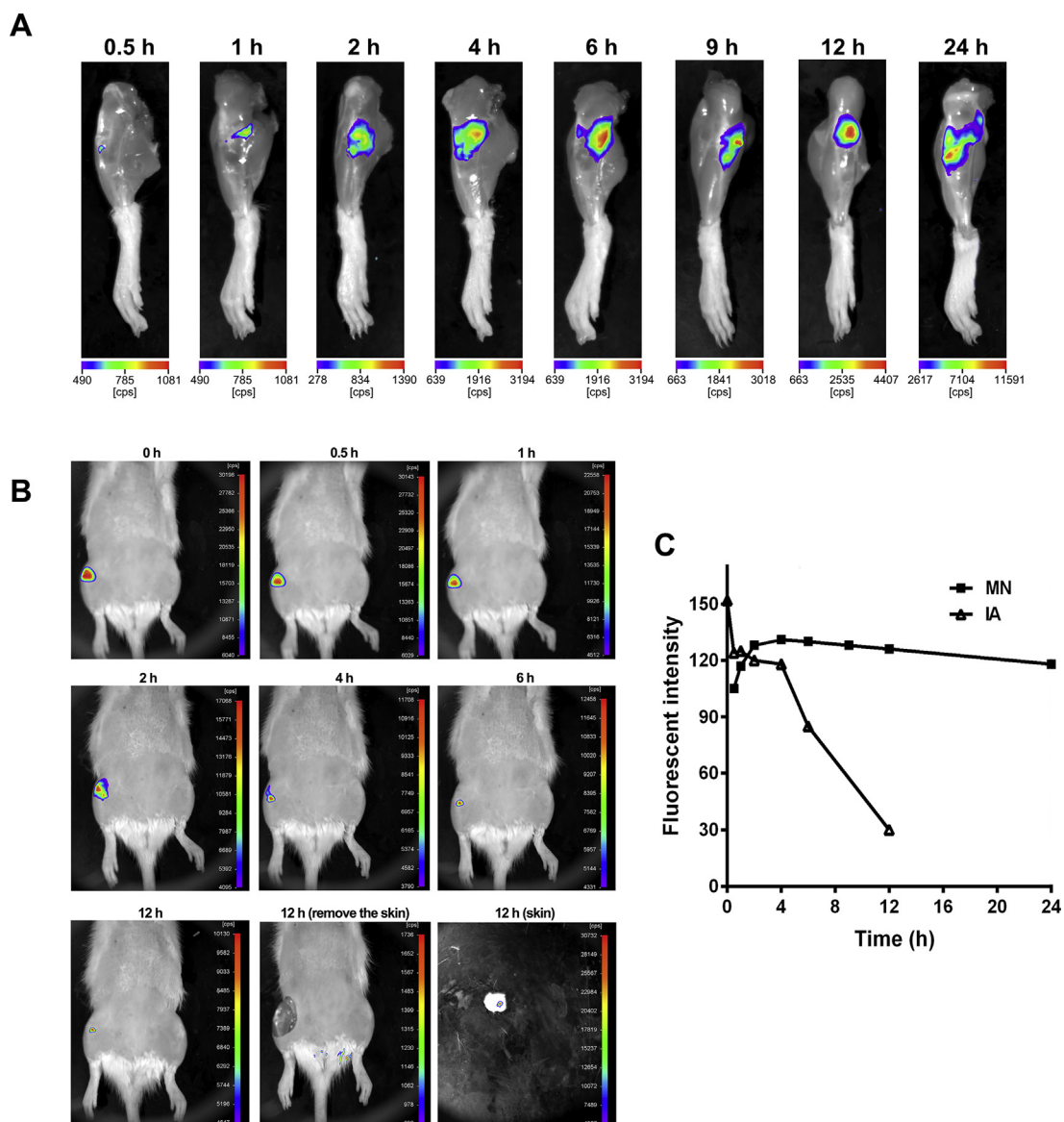
Figure 6 *In vivo* imaging of rat knees after treated with layered MNs and intra-articular injection. *In vivo* images of RhB delivery from layered MNs into the articular cavity of rats throughout 24 h (A); RhB in the articular cavity of rats *via* intra-articular injection throughout 12 h (B); and the fluorescence intensity with time (C). In the layered MNs treated group, the treated skin covering the articular cavity was removed prior to imaging at each time point; while the treated skin in the intra-articular injection group was removed at 12 h post-injection.

higher TAC skin retention than that of un-layered MNs (MIX-MN), resulting in better anti-psoriatic effects. Finally, the MNs could lower the TEWL value and restore skin barrier function to some extent. Recovery of skin lesions involves hemostasis, inflammation, proliferation, and remodeling, but the stagnation of inflammation often occurs. MN insertion into the skin could produce slight inflammation and stimulate the migration of epithelial cells to skin lesions, causing the acceleration of skin from the inflammatory phase to the proliferative phase and then promote the recovery of skin barrier function[34], thereby effectively alleviating erythema and hemorrhage and accelerating scabs and scale shedding in the treatment of psoriasis-like lesions. Moreover, HA, as the main component of the MN formulations, is an endogenous substance of the epidermis and dermis, that can maintain cell moisture, promote cell migration, and improve the healing ability of skin lesions[49,50].

PsA has a variety of phenotypes, among which rheumatoid arthritis (RA) is common. Due to similar immune disorders between PsA and RA, RA animal models are usually used to investigate therapeutic effects on PsA in numerous studies[51]. Carrageenan-induced arthritic rats possess many symptoms analogous to human RA, such as synovitis, the formation of synovial vessels, and degradation of matrix proteoglycan in articular cartilage[44]. A schematic diagram of arthritis model establishment and the treatment protocol is shown in Fig. 8A and B, respectively. Knee joint inflammation was evaluated by measuring the knee diameter and calculating the swelling degree as a direct index of arthritis[52], and muscle atrophy was a subsequent index of arthritis. Effective treatment can reduce swelling and prevent muscle atrophy of the affected knee. As expected, one day after injection of λ-carrageenan and kaolin into the right synovial cavity, the affected knee presented marked swelling. Compared to the normal
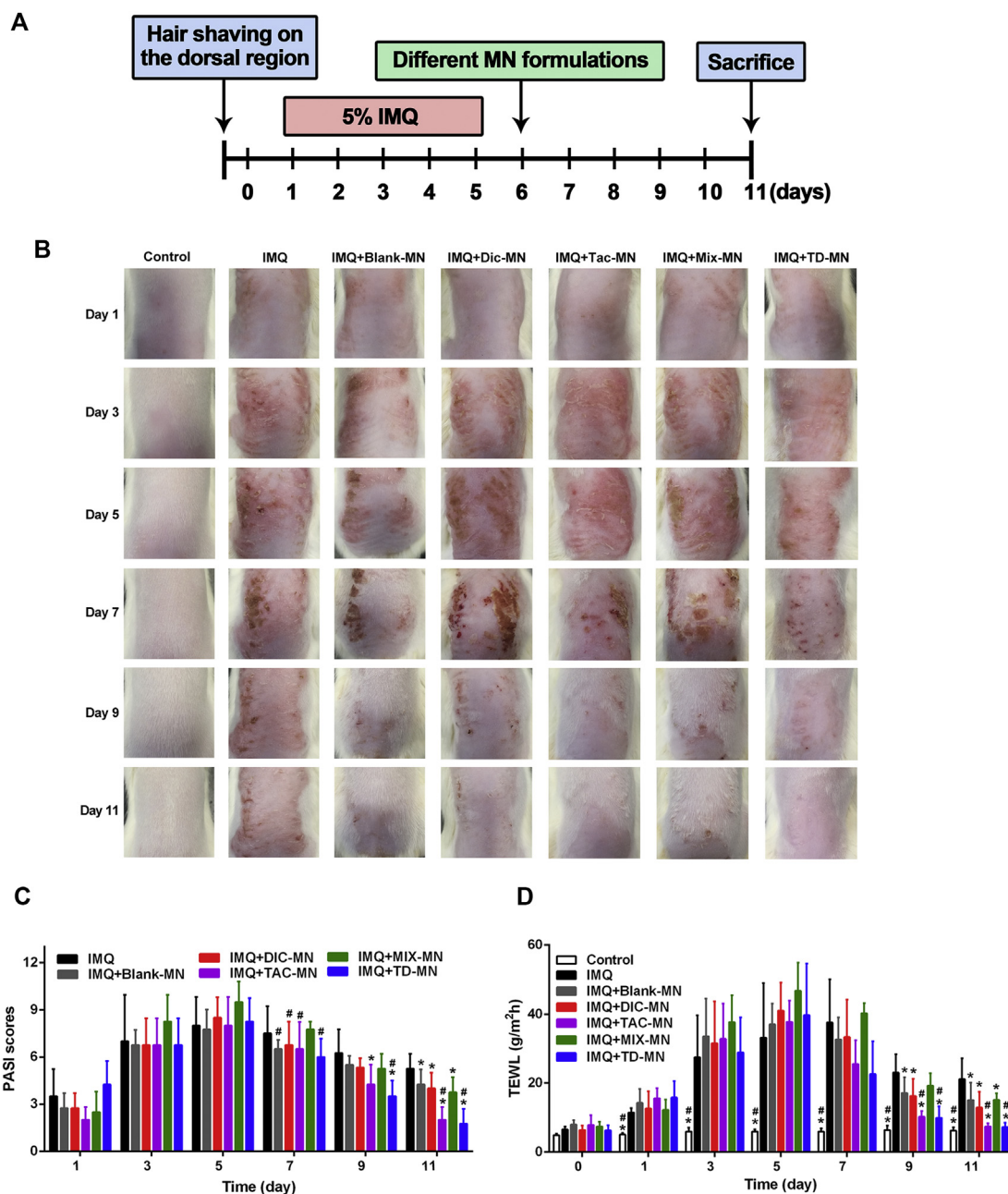
Figure 7 Psoriasis model establishment and treatment. Schematic diagram of protocols of IMQ-induced psoriasis rat model establishment and the treatment (A). The representative skin clinical manifestations throughout model establishment and treatment (B). PASI scores of psoriatic skin lesions treated with different MN formulations (C). TEWL of psoriatic skin lesions treated with different MN formulations (D). Each symbol and bar represented the mean±standard derivation of six determinations. Significant differences were calculated using ANOVA test. *$P < 0.05$ in comparison with the IMQ group; #$P < 0.05$ in comparison with the IMQ+MIX-MN group.

left knee joint, the swelling degree was ∼25%, indicating the successful establishment of the arthritis model. After treatment with different formulations, the changes in the swelling degree during the experiment are presented as shown in Fig. 8C. In contrast to the anti-psoriatic experiment, blank-MN presented no significant effect on reducing the swelling of arthritis throughout treatment compared with the model group, while, the other formulations containing drugs alleviated the arthritis to different levels. DIC-injection, DIC-MN, and TD-MN took effect quicker than the other formulations; they significantly reduced the swelling starting on Day 3, and the swelling sustainably decreased

with time. However, MIX-MN and TAC-MN significantly reduced swelling beginning on Day 5. Importantly, recurrent swelling occurred in the DIC-injection group on Day 7, indicating that a higher frequency of DIC-injection is necessary to treat arthritis, which is consistent with the results from the *in vivo* visualization of drug distribution in the articular cavity. Intra-articular injection of DIC could immediately reach the articular cavity but quickly distribute systemically and then be metabolized, and the DIC concentration in the inflamed joints consequently decreased. TD-MN and DIC-MN showed a sustained reduction in the swelling throughout the experiment and the results were better than
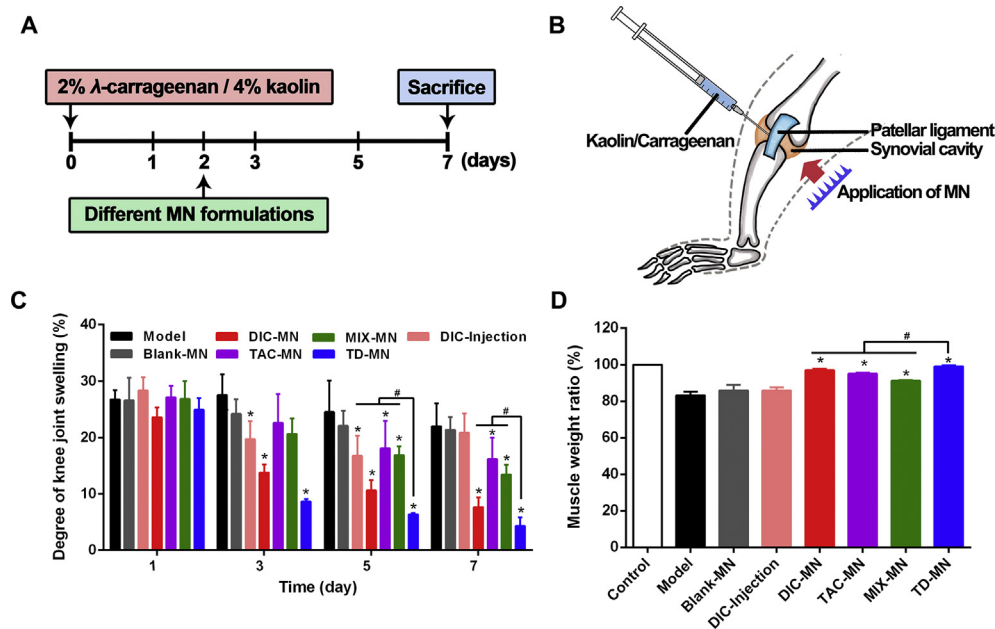
Figure 8 Arthritis model establishment and treatment. Schematic diagram of protocols of carrageenan/kaolin-induced arthritis rat model establishment and treatment (A and B). Degree of knee joint swelling after treated with different MN formulations throughout the experiment (C). Muscle weight ratio after treated with different MN formulations (D). Each symbol and bar represented the mean±standard derivation of six determinations. Significant differences were calculated using ANOVA test. *$P < 0.05$ in comparison with the IMQ group; #$P < 0.05$ in comparison with TD-MN group.

those of MIX-MN and TAC-MN. Interestingly, TD-MN presented the strongest anti-swelling effects among the MN formulations, and the swelling degree decreased to ~4.33%. Prevention of muscle atrophy after treatment with different formulations is shown in Fig. 8D. Compared with the model group, both blank-MN and DIC-injection could not prevent muscle atrophy of the affected knee. MN formulations containing drugs significantly prevented muscle atrophy, and TD-MN performed better than DIC MN, TAC-MN, and MIX-MN ($P < 0.05$). The results are as follows. First, TD-MN and DIC-MN had significantly better therapeutic effects compared with the other groups. DIC loaded in TD-MN and DIC-MN played a major role in the treatment of arthritic rats. As a potent NSAID, DIC dramatically inhibited joint swelling and lowered the risk of muscle atrophy. However, when DIC was injected intra-articularly, its anti-inflammatory effect was not sustained, and frequent injection was necessary for arthritis clinical requirements. While TD-MN or DIC-MN pierced the skin, DIC loaded in the tip-layer of the needle was partially directly delivered into the articular cavity, and the remaining DIC displayed sustained release from the needle tip reservoir supplied into the articular cavity. The pharmacodynamic effects of anti-swelling and atrophy confirmed the results from the *in vitro* and *in vivo* permeation and drug distribution experiments. Second, TD-MN was superior to DIC-MN with respect to anti-swelling and atrophy, and TAC-MN also had a marked therapeutic effect against arthritis. TAC has been demonstrated to have anti-arthritic effects by effectively inhibiting inflammation and the expression of TNF-α and IL-1β in rodents[53,54], thereby alleviating bone and cartilage lesions. DIC and TAC in TD-MN might have a synergistic effect for the treatment of arthritis; thus, the anti-arthritic effects of TD-MN were better than those of DIC-MN.

Comprehensively, considering the therapeutic effects of the layered MNs in psoriasis and arthritis animal models, it was found that the layered MNs had stronger effects on inhibiting disease development than the other MN groups, which achieved the proof of concept of a TAC and DIC need-based delivery system of for the simultaneous alleviation of skin and joint lesions in PsA.

3.6.2. Histopathological analysis
H&E staining of psoriasis-like skin induced by IMQ revealed histological changes in epidermal thickening[55]. As shown in Fig. 9, the epidermis of psoriatic skin induced by IMQ present marked hyperkeratosis, which is significantly thicker than that of the normal epidermis (87.97 ± 18.44 vs. 25.45 ± 3.15 μm, $P < 0.05$), and serious infiltration of lymphocytes is observed in the dermis. After treatment with different MN formulations, the thickened epidermis recovered compared with the IMQ group ($P < 0.05$); even Blank-MN presented decreased epidermal thickness. HA-based MNs probably increase skin hydration, resulting in amelioration of the dryness and scaling produced by IMQ application. Additionally, TD-MN and TAC-MN further ameliorated the thickened epidermis compared with the other drug-loaded MN groups. Overall, TD-MN, similar to TAC-MN, exhibited minimal epidermal thickening compared to the negative control.

H&E and safranin O-fast green staining of λ-carrageenan/kaolin-induced arthritis of the knee joint in rats was performed to observe histological changes, including cartilage erosion, synovitis, and infiltration of inflammatory cells (Fig. 11). The knee joint of the model group displays the typical histological manifestations of arthritis with rough articular cartilage surface, disordered arrangement of chondrocytes, and infiltration of numerous inflammatory cells in synovial tissue (Fig. 10A). Safranin O is an alkaline dye that marks cartilage red, and fast green is an acidic dye that combines with subchondral bone to show a green color. The loss of red represents cartilage degradation. A large loss of safranin-stained area appears in the articular cartilage of the model group (Fig. 10B), which indicated the

increased degradation of proteoglycan and severe cartilage destruction. Except for Blank-MN and DIC-injection, the pathological manifestations of arthritis had different degrees of mitigation after treatment with different drug-loaded MN formulations, similar to the results above. However, treatment with TD-MN presented the best alleviation effects on cartilage destruction and bone erosion compared with other drug-loaded MN formulations. DIC-injection could not alleviate the pathological manifestations of arthritis because the recurrent swelling occurred in the DIC-injection group on Day 7, as described in Section 3.6.1.

3.6.3. TD-MN inhibits serum pro-inflammatory cytokines

TNF-α is the central cytokine in the development of many autoimmune diseases, and has become an important target for the treatment of psoriasis and arthritis[56]. Anti-TNF-α biologics, novel medications for psoriasis, arthritis, and PsA, have been widely used in the clinic. During the pathogenesis of psoriasis, TNF-α secreted by activated T cells and antigen-presenting cells cannot trigger keratinocyte reaction alone but has strong synergistic effects when combined with IL-17A, IL-17C or other cytokines, which sets off a cytokine storm and aggravates the inflammatory process of psoriasis[57]. Furthermore, the increased expression of IL-17A has been determined in psoriasis and other autoimmune diseases, including rheumatoid arthritis and systemic lupus erythematosus[58,59]. Therefore, in this study, serum TNF-α and IL-17A levels in psoriatic and arthritic rats were determined to further investigate the therapeutic effects of different MN formulations on reducing pro-inflammatory cytokines. As shown in Fig. 11, serum TNF-α and IL-17A levels of our IMQ-induced psoriatic and λ-carrageenan and kaolin-induced arthritic rats are markedly higher than the normal levels of the negative control ($P < 0.05$). After treatment with different MN formulations, serum TNF-α levels significantly decreased. It is noteworthy that serum TNF-α levels were downregulated to a level comparable to the normal level after the psoriatic rats were treated with TAC-MN or TD-MN and the arthritic rats were treated with DIC-MN or TD-MN, and significantly lower than those of the MIX-MN-treated rats ($P < 0.05$). The results are consistent with those of general observations and the histopathological analysis. However, for IL-17A, only TAC-MN and TD-MN significantly inhibited its elevation in psoriatic rats ($P < 0.05$), and there was no significant difference between the negative control and TD-MN-treated group. Additionally, only DIC-MN and TD-MN significantly inhibited IL-17A elevation in arthritic rats ($P < 0.05$). Nevertheless, the other formulations did not significantly decrease IL-17A levels. In the pathogenesis of both psoriasis and arthritis, the powerful synergism between TNF-α and IL-17A is attributed to the stabilization of TNF-α on IL-17A mRNA, and TNF-α could potentiate IL-17A[60]. After the psoriatic rats were treated with
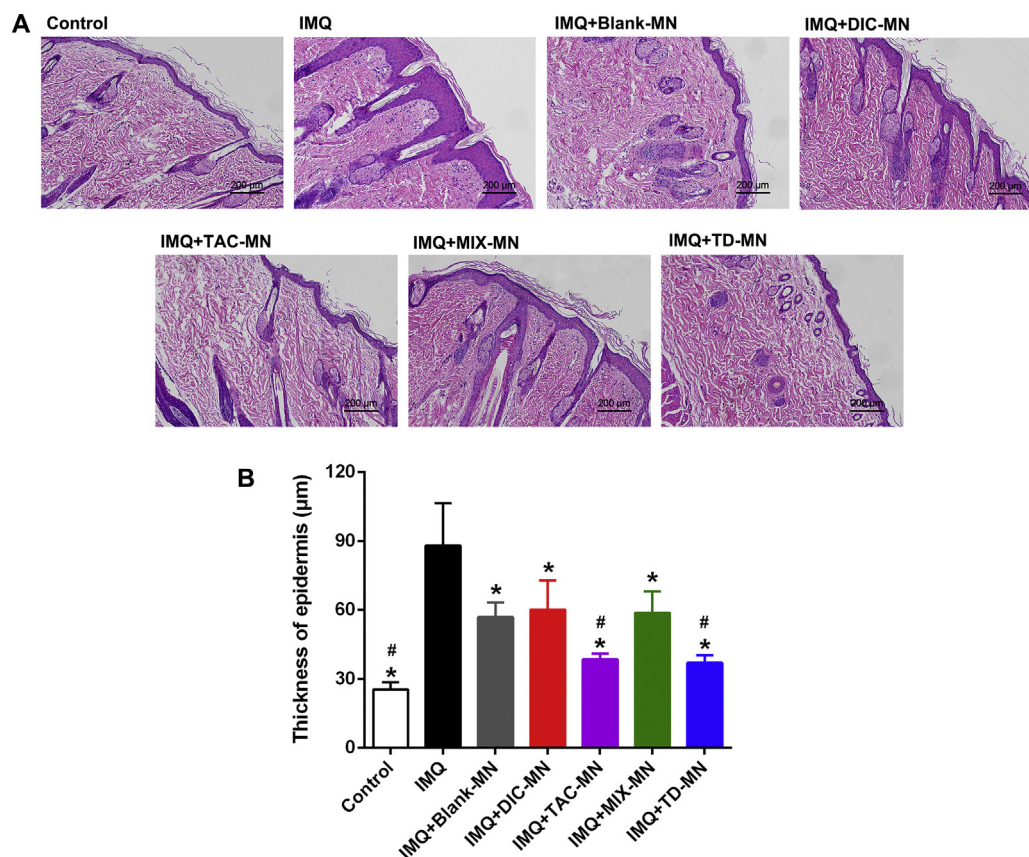
Figure 9 Histopathological analysis of the psoriatic rats treated with different MN formulations. Histological analysis of skin after 5 days of anti-psoriatic treatment with different MN formulations (A). The epidermal thickness of skin measured under the microscope (B). The sliced sections were stained with hematoxylin and eosin (magnification 100×). Scale bar $= 200$ μm. Mean of epidermal thickness was calculated based on 20 random site measurements. Significant differences were calculated using ANOVA test. *$P < 0.05$ in comparison with the IMQ group; #$P < 0.05$ in comparison with the IMQ+MIX-MN group.
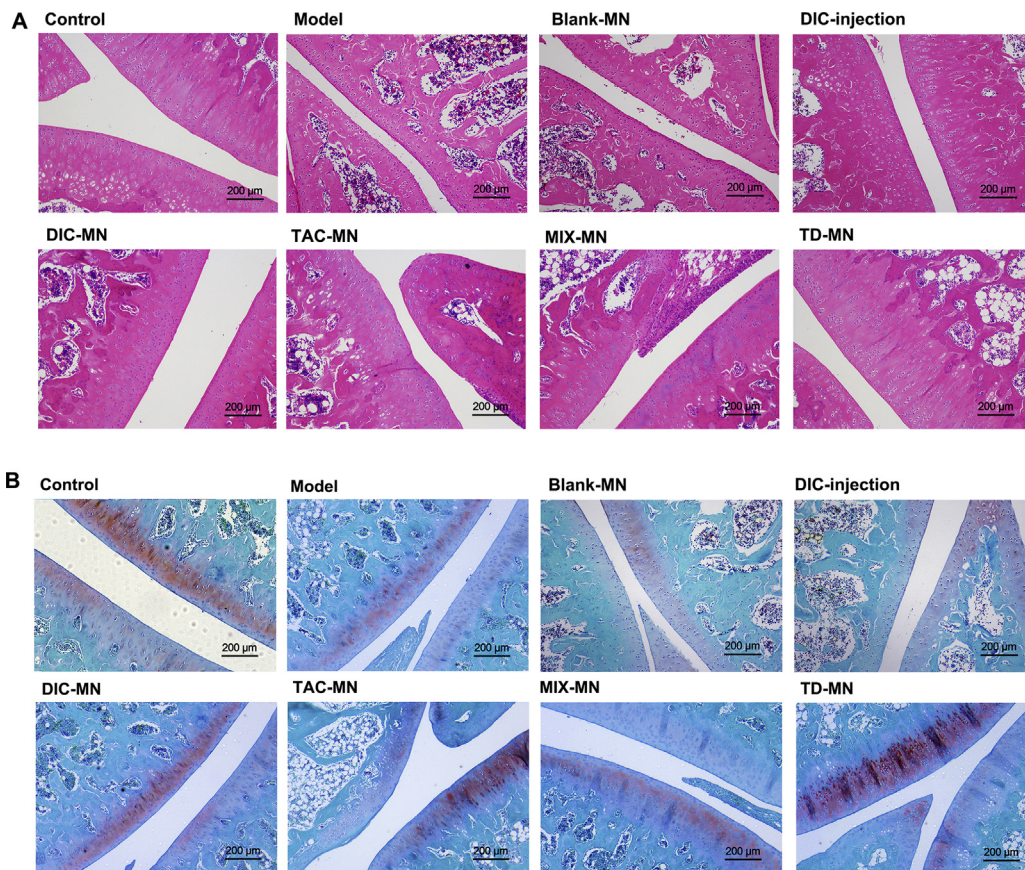
Figure 10 Histopathological analysis of the arthritic rats treated with different MN formulations. Histological analysis of knee joint after 5 days of anti-arthritic treatment with different MN formulations. The sliced sections were stained with hematoxylin and eosin (A) and safranin O-fast green (B) (magnification 100×). Scale bar = 200 μm.
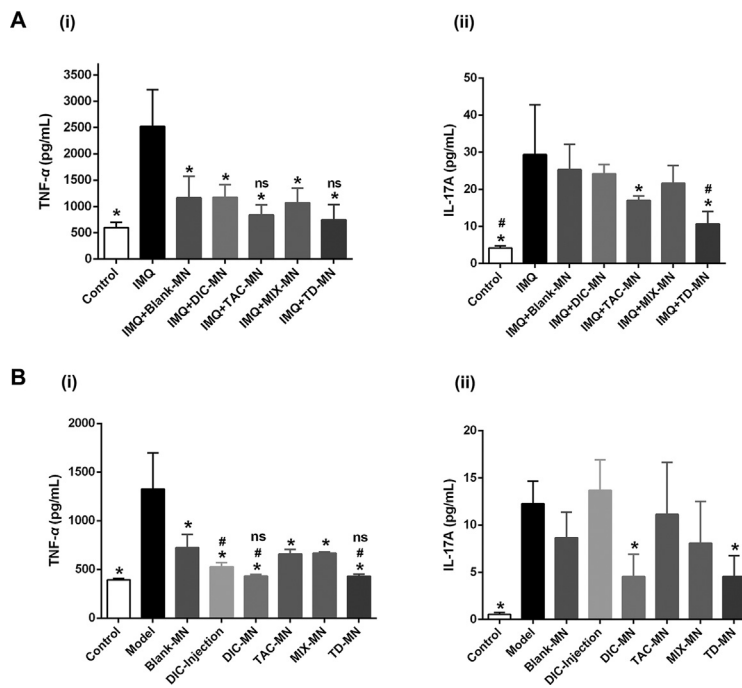
Figure 11 Effects of different MN formulations on serum TNF-α (i) and IL-17A (ii) levels in psoriatic (A) and arthritic (B) rats. Each symbol and bar represented mean±standard derivation of six determinations. Significant differences were calculated using ANOVA test. *$P < 0.05$ in comparison with the positive group (IMQ-induced psoriatic and carrageenan/kaolin-induced arthritic model group); #$P < 0.05$ in comparison with MIX-MN group; ns, no significant difference with the negative group.

TAC-MN or TD-MN or the arthritic rats were treated with DIC-MN or TD-MN, the serum TNF-α in psoriatic or arthritic animals recovered to normal levels, therefore, the normal level of TNF-α was unable to potentiate IL-17A and the synergism between TNF-α and IL-17A was blocked. Consequently, TD-MN was comparable to TAC-MN for psoriatic rats and to DIC-MN for arthritic rats and significantly inhibited TNF-α and IL-17A. This inhibition is its underlying mechanism of therapeutic action against PsA. In short, as expected, taken together, general observations, histopathological analysis, and pro-inflammatory cytokine determination, MNs layered-loaded with TAC and DIC can kill two birds with one stone by simultaneously alleviating joint and skin lesions in PsA treatment.

4. Conclusions

PsA is a complicated psoriasis comorbidity with both skin and joint lesions, and its effective treatment should alleviate skin and joint symptoms simultaneously. In this study, we developed a layered MN as a percutaneous layer-loaded system with TAC and DIC for PsA treatment, which consisted of inter-layer loading of TAC and tip-layer loading of DIC. *In vitro* and *in vivo* skin permeation studies demonstrated that the inter-layer retained TAC within the superficial skin while the tip-layer delivered DIC into the articular cavity, and both deliveries were significantly higher than those of MIX-MN. The therapeutic efficacy of TAC and DIC layer-loaded by MNs was comparable to TAC-MN against psoriasis and comparable to DIC-MN against arthritis, and was even better than DIC-injection. Therefore, layered MNs were advantageous in enhancing the permeability and efficacy of the drugs, avoiding the possible risk of systemic side effects caused by oral administration and frequent intra-articular injection, thereby leading to better patient compliance. Overall, layer-loaded TAC and DIC in our layered MNs can deliver need-based TAC and DIC to the psoriatic skin and arthritic articular cavity, respectively, simultaneously treating skin and joint lesions in PsA. Therefore, this approach represents a promising alternative to the multi-administration of different drugs for comorbidity, providing a convenient and effective strategy that meets the requirements of PsA treatment.

Author contributions

Kaiyue Yu and Yuehong Xu designed the research. Kaiyue Yu, Xiuming Yu, and Sisi Cao carried out the experiments and performed data analysis. Yixuan Wand, Yuanhao Zhai, and Fengdie Yang participated part of the experiments. Xiaoyuan Yang and Yi Lu Yi provided experimental drugs and quality control. Kaiyue Yu and Xiuming Yu wrote the manuscript. Yuehong Xu and Chuanbin Wu revised the manuscript. All of the authors have read and approved the final manuscript.

Conflicts of interest

The authors have no conflicts of interest to declare.

References

1. Sala M, Elaissari A, Fessi H. Advances in psoriasis physiopathology and treatments: up to date of mechanistic insights and perspectives of novel therapies based on innovative skin drug delivery systems (ISDDS). *J Control Release* 2016;**239**:182−202.
2. Boehncke WH, Schön MP. Psoriasis. *Lancet* 2015;**386**:983−94.
3. Bata-Csorgo Z, Hammerberg C, Voorhees JJ, Cooper KD. Flow cytometric identification of proliferative subpopulations within normal human epidermis and the localization of the primary hyperproliferative population in psoriasis. *J Exp Med* 1993;**178**:1271−81.
4. Nestle FO, Kaplan DH, Barker J. Psoriasis. *N Engl J Med* 2009;**361**: 496−509.
5. Ritchlin CT, Proulx S, Schwarz ES. Translational perspectives on psoriatic arthritis. *J Rheumatol Suppl* 2009;**83**:30−4.
6. Ibrahim G, Waxman R, Helliwel PS. The prevalence of psoriatic arthritis in people with psoriasis. *Arthritis Rheum* 2009;**61**:1373−8.
7. Ritchlin CT, Colbert RA, Gladman DD. Psoriatic arthritis. *N Engl J Med* 2017;**376**:957−70.
8. Caso F, Navarini L, Ruscitti P, Chimenti MS, Girolimetto N, Puente AD, et al. Targeted synthetic pharmacotherapy for psoriatic arthritis: state of the art. *Expet Opin Pharmacother* 2020;**21**:785−96.
9. Menter A, Korman NJ, Elmets CA, Freldman CA, Gelfand SR, Gordon KB, et al. Guidelines of care for the management of psoriasis and psoriatic arthritis: section 3. Guidelines of care for the management and treatment of psoriasis with topical therapies. *J Am Acad Dermatol* 2009;**60**:643−59.
10. Gossec L, Smolen JS. Treatment of psoriatic arthritis: management recommendations. *Clin Exp Rheumatol* 2015;**33**:S73−7.
11. Chang K, Lin H, Kuo C, Hung C. Tacrolimus suppresses atopic dermatitis-associated cytokines and chemokines in monocytes. *J Microbiol Immunol Infect* 2016;**49**:409−16.
12. Malecic N, Young H. Tacrolimus for the management of psoriasis: clinical utility and place in therapy. *Psoriasis (Auckl)* 2016;**6**:153−63.
13. Brune A, Miller DW, Lin P, Cotrim-Russi D, Paller AS. Tacrolimus ointment is effective for psoriasis on the face and intertriginous areas in pediatric patients. *Pediatr Dermatol* 2007;**24**:76−80.
14. Furst DE, Saag K, Fleischmann MR, Sherrer Y, Block JA, Schnitzer T, et al. Efficacy of tacrolimus in rheumatoid arthritis patients who have been treated unsuccessfully with methotrexate: a six-month, double-blind, randomized, dose-ranging study. *Arthritis Rheum* 2002;**46**:2020−8.
15. Gossec L, Smolen JS, Ramiro S, de Wit M, Cutolo M, Dougados M, et al. European League against Rheumatism (EULAR) recommendations for the management of psoriatic arthritis with pharmacological therapies: 2015 update. *Ann Rheum Dis* 2016;**75**:499−510.
16. Singh JA, Guyatt G, Ogdie A, Gladman DD, Deal C, Deodhar A, et al. Special article: 2018 American College of Rheumatology/National Psoriasis Foundation guideline for the treatment of psoriatic arthritis. *Arithritis Rheumatol* 2019;**71**:5−32.
17. Warner TD, Giuliano F, Vojnovic I, Bukasa A, Mitchell JA, Vane JR. Nonsteroid drug selectivities for cyclo-oxygenase-1 rather than cyclo-oxygenase-2 are associated with human gastrointestinal toxicity: a full *in vitro* analysis. *Proc Natl Acad Sci U S A* 1999;**96**:7563−8.
18. Gan TJ. Diclofenac: an update on its mechanism of action and safety profile. *Curr Med Res Opin* 2010;**26**:1715−31.
19. Mertz N, Larsen SW, Kristensen J, Østergaard J, Larsen C. Long-acting diclofenac ester prodrugs for joint injection: kinetics, mechanism of degradation, and *in vitro* release from prodrug suspension. *J Pharm Sci* 2016;**105**:3079−87.
20. Elron-Gross I, Glucksam Y, Biton IE, Margalit R. A novel diclofenac-carrier for local treatment of osteoarthritis applying live-animal MRI. *J Control Release* 2009;**135**:65−70.
21. Prausnitz MR. Microneedles for transdermal drug delivery. *Adv Drug Deliv Rev* 2004;**56**:581−7.
22. Rzhevskiy AS, Singh TRR, Donnelly RF, Anissimov YG. Microneedles as the technique of drug delivery enhancement in diverse organs and tissues. *J Control Release* 2018;**270**:184−202.

23. Jin X, Zhu DD, Chen BZ, Ashfaq M, Guo XD. Insulin delivery system combined with microneedle technology. *Adv Drug Deliv Rev* 2018; **127**:119−37.

24. Rodgers AM, Cordeiro AS, Kissenpfennig A, Donnelly R. Microneedle arrays for vaccine delivery: the possibilities, challenges and use of nanoparticles as a combinatorial approach for enhanced vaccine immunogenicity. *Expet Opin Drug Deliv* 2018;**15**:851−67.

25. Du H, Liu P, Zhu J, Lan J, Li Y, Zhang L, et al. Hyaluronic acid-based dissolving microneedle patch loaded with methotrexate for improved treatment of psoriasis. *ACS Appl Mater Interfaces* 2019;**11**:43588−98.

26. Sabri AH, Ogilvie J, Abdulhamid K, Shpadaruk V, McKenna J, Segal J, et al. Expanding the applications of microneedles in dermatology. *Eur J Pharm Biopharm* 2019;**140**:121−40.

27. Lee JH, Jung YS, Kim GM, Bae JM. A hyaluronic acid-based microneedle patch to treat psoriatic plaques: a pilot open trial. *Br J Dermatol* 2018;**178**:e24−5.

28. Chen G, Chen Z, Wen D, Wang Z, Li H, Zeng Y, et al. Transdermal cold atmospheric plasma-mediated immune checkpoint blockade therapy. *Proc Natl Acad Sci U S A* 2020;**117**:3687−92.

29. Ye Y, Wang J, Hu Q, Hochu GM, Xin H, Wang C, et al. Synergistic transcutaneous immunotherapy enhances antitumor immune responses through delivery of checkpoint inhibitors. *ACS Nano* 2016;**10**: 8956−63.

30. Yao W, Tao C, Zou J, Zheng H, Zhu J, Zhu Z, et al. Flexible two-layer dissolving and safing microneedle transdermal of neurotoxin: a biocomfortable attempt to treat Rheumatoid Arthritis. *Int J Pharm* 2019; **563**:91−100.

31. Zhang Q, Xu C, Lin S, Zhou H, Yao G, Liu H, et al. Synergistic immunoreaction of acupuncture-like dissolving microneedles containing thymopentin at acupoints in immune-suppressed rats. *Acta Pharm Sin B* 2018;**8**:449−57.

32. Yang J, Liu X, Fu Y, Song Y. Recent advances of microneedles for biomedical applications: drug delivery and beyond. *Acta Pharm Sin B* 2019;**9**:469−83.

33. Ye Y, Yu J, Wen D, Kahkoska AR, Gu Z. Polymeric microneedles for transdermal protein delivery. *Adv Drug Deliv Rev* 2018;**127**:106−18.

34. Liebl H, Kloth LC. Skin cell proliferation stimulated by microneedles. *J Am Coll Clin Wound Spec* 2012;**4**:2−6.

35. Pan J, Ruan W, Qin M, Long Y, Wan T, Yu K, et al. Intradermal delivery of STAT3 siRNA to treat melanoma *via* dissolving microneedles. *Sci Rep* 2018;**8**:1117.

36. Pan W, Qin M, Zhang G, Long Y, Ruan W, Wu Z, et al. Combination of hydrotropic nicotinamide with nanoparticles for enhancing tacrolimus percutaneous delivery. *Int J Nanomed* 2016;**11**:4037−50.

37. Lin S, Quan G, Hou A, Yang P, Peng T, Gu Y, et al. Strategy for hypertrophic scar therapy: improved delivery of triamcinolone acetonide using mechanically robust tip-concentrated dissolving microneedle array. *J Control Release* 2019;**306**:69−82.

38. Migdadi EM, Courtenay AJ, Tekko IA, McCrudden MTC, Kearney MC, McAlister E, et al. Hydrogel-forming microneedles enhance transdermal delivery of metformin hydrochloride. *J Control Release* 2018;**285**:142−51.

39. Larraneta E, Moore J, Vicente-Pérez EM, González-Vázquezet P, Lutton R, Woolfson AD, et al. A proposed model membrane and test method for microneedle insertion studies. *Int J Pharm* 2014;**472**:65−73.

40. Flores RR, Carbo L, Kim E, Meter MV, Lopez De Padilla CM, Zhao J, et al. Adenoviral gene transfer of a single-chain IL-23 induces psoriatic arthritis-like symptoms in NOD mice. *Faseb J* 2019;**33**:9505−15.

41. Okasha EF, Bayomy NA, Abdelaziz EZ. Effect of topical application of black seed oil on imiquimod-induced psoriasis-like lesions in the thin skin of adult male albino rats. *Anat Rec* 2018;**301**:166−74 (Hoboken).

42. Satake K, Amano T, Okamoto T. Low systemic exposure and calcemic effect of calcipotriol/betamethasone ointment in rats with imiquimod-induced psoriasis-like dermatitis. *Eur J Pharmacol* 2018;**826**:31−8.

43. Kim KS, Kim MH, Yeom M, Choi HM, Yang H, Yoo MC, et al. Arthritic disease is more severe in older rats in a kaolin/carrageenan-induced arthritis model. *Rheumatol Int* 2012;**32**:3875−9.

44. Vargas-Ruiz R, Montiel-Ruiz RM, Herrera-Ruiz M, González-Cortazar M, Ble-González EA, Jiménez-Aparicio AR, et al. Effect of phenolic compounds from *Oenothera rosea* on the kaolin-carrageenan induced arthritis model in mice. *J Ethnopharmacol* 2020;**253**:112711.

45. Kim H, Thompson J, Ji G, Ganapathy V, Neugebauer V. Monomethyl fumarate inhibits pain behaviors and amygdala activity in a rat arthritis model. *Pain* 2017;**158**:2376−85.

46. Sun L, Liu Z, Wang L, Cun D, Tong HHY, Yan R, et al. Enhanced topical penetration, system exposure and anti-psoriasis activity of two particle sized, curcumin-loaded PLGA nanoparticles in hydrogel. *J Control Release* 2017;**254**:44−54.

47. Zhao X, Li X, Zhang P, Du J, Wang Y. Tip-loaded fast-dissolving microneedle patches for photodynamic therapy of subcutaneous tumor. *J Control Release* 2018;**286**:201−9.

48. Mwangi TK, Berke IM, Nieves EH, Bell RD, Asams SB, Setton LA. Intra-articular clearance of labeled dextrans from naive and arthritic rat knee joints. *J Control Release* 2018;**283**:76−83.

49. Huynh A, Priefer R. Hyaluronic acid applications in ophthalmology, rheumatology, and dermatology. *Carbohydr Res* 2020;**489**: 107950.

50. Zhu J, Tang X, Jia Y, Ho C, Huang Q. Applications and delivery mechanisms of hyaluronic acid used for topical/transdermal delivery—a review. *Int J Pharm* 2020;**578**:119127.

51. Coates LC, FitzGerald O, Helliwell PS, Paul C. Psoriasis, psoriatic arthritis, and rheumatoid arthritis: is all inflammation the same?. *Semin Arthritis Rheum* 2016;**46**:291−304.

52. Shi Y, Xie F, Rao P, Qian H, Chen R, Chen H, et al. TRAIL-expressing cell membrane nanovesicles as an anti-inflammatory platform for rheumatoid arthritis therapy. *J Control Release* 2020; **320**:304−13.

53. Sakuma S, Kato Y, Nishigaki F, Sasakawa T, Magari K, Miyata S, et al. FK506 potently inhibits T cell activation induced TNF-alpha and IL-1beta production *in vitro* by human peripheral blood mononuclear cells. *Br J Pharmacol* 2000;**130**:1655−63.

54. Magari K, Nishigaki F, Sasakawa T, Ogawa T, Miyata S, Ohkubo Y, et al. Anti-arthritic properties of FK506 on collagen-induced arthritis in rats. *Inflamm Res* 2003;**52**:524−9.

55. Dolz-Pérez I, Sallam MA, Masiá E, MorellÓ-Bolumar D, Del Caz MDP, Graff P, et al. Polypeptide-corticosteroid conjugates as a topical treatment approach to psoriasis. *J Control Release* 2020;**318**:210−22.

56. Baliwag J, Barnes DH, Johnston A. Cytokines in psoriasis. *Cytokine* 2015;**73**:342−50.

57. Chiricozzi A, Guttman-Yassky E, Suárez-Fariñas M, Nograles KE, Tian S, Cardinale I, et al. Integrative responses to IL-17 and TNF-α in human keratinocytes account for key inflammatory pathogenic circuits in psoriasis. *J Invest Dermatol* 2011;**131**:677−87.

58. Kryczek I, Bruce AT, Gudjonsson JE, Johnston A, Aphale A, Vatan L, et al. Induction of IL-17^{+} T cell trafficking and development by IFN-gamma: mechanism and pathological relevance in psoriasis. *J Immunol* 2008;**181**:4733−41.

59. Zhu S, Qian Y. IL-17/IL-17 receptor system in autoimmune disease: mechanisms and therapeutic potential. *Clin Sci* 2012;**122**:487−511 (Lond).

60. Hartupee J, Liu C, Novotny M, Li X, Hamilton T. IL-17 enhances chemokine gene expression through mRNA stabilization. *J Immunol* 2007;**179**:4135−41.